

温度驱动飞秒激光打印微结构的可逆自组装

倪才鼎¹, 劳召欣^{2*}, 任中国¹, 陈超³, 吴东¹¹中国科学技术大学工程科学学院, 安徽 合肥 230026;²合肥工业大学仪器科学与光电工程学院测量理论与精密仪器安徽省重点实验室, 安徽 合肥 230009;³合肥工业大学材料科学与工程学院材料物理及新能源材料与器件系, 安徽 合肥 230009

摘要 模板引导的毛细力驱动自组装技术逐渐被认为是制造一系列微纳米结构的一种替代方法。毛细力自组装结构的稳定性取决于结构接触力和支撑力的竞争, 接触面积越大, 接触力越大。当接触面积大于临界值时, 微结构的组装行为不可逆。利用飞秒激光打印具有各向异性的微结构, 在不同温度的调控下实现其多方向运动, 并借助温度响应水凝胶的反向变形能力, 实现了线接触微结构的可逆自组装。此外还探究了该方法在微执行器、微传感器方向的应用。结果表明, 通过改变环境的温度能够实现微结构的弯曲变形, 且利用飞秒激光双光子加工的灵活性和毛细力驱动的简便性, 可以实现可逆变形的微图案以及功能丰富的微传感结构。

关键词 激光技术; 飞秒激光; 双光子聚合; 毛细力; 自组装; 温度响应

中图分类号 O436 文献标志码 A

DOI: 10.3788/CJL230651

1 引言

飞秒激光直写是一种自上而下的微纳加工技术, 具有真三维、分辨率高以及适用材料范围广等优点, 基于加工材料的双光子效应, 能够实现空间任意轨迹的可控加工, 目前该技术被广泛应用于微机械^[1]、微光学器件^[2-3]、微流控^[4-5]以及生物医学^[6-7]等领域。但是飞秒激光直写采用逐点加工的方式, 制备复杂层级结构时就必然会出现加工费时问题, 所以时间问题亟待解决。而毛细力驱动自组装是一种常用的自下而上的微纳制备技术^[8-10], 可以高效快速地制备大量微纳结构, 但可控性差。因此, 为了制备大面积且可控的复杂多层级结构, 将飞秒激光加工和毛细力驱动组装技术结合已成为引人关注的微纳加工手段。利用飞秒激光打印和毛细力驱动自组装(LPCS)技术, 可以高效稳定制备有序的多层级结构, 实现微物体的选择性捕获和释放^[11]。通过在柔性基底上制备可调节间距的微组装体, 可实现精确捕获^[12]。利用LPCS制备纳米间隙等离子体结构, 可检测表面增强拉曼散射(SERS)^[13-14]。除此之外, 还可以制备自封闭的微墙结构, 在毛细力的驱动下获得具有超长尺寸的毛细血管通道^[15]。在LPCS方法中, 毛细力驱动基元自组装为多层级结构, 结构稳定性取决于结构间接触力(如范德瓦耳斯力)和结构弹性力之间的竞争。而结构间接触力与结构的接触面积正相关, 接触面积越大, 结构接触力也就越大,

相应地, 结构越稳定。课题组前期研究发现, 对于线接触甚至面接触的微墙等结构, 在组装闭合后接触区域过大导致液体分子浸入后无法恢复直立状态, 这在很大程度上限制了结构的应用范围。因此, 对于线(面)接触的结构, 需要找到一种制备方式以实现结构的可逆调控。

线接触区域的范德瓦耳斯力过大导致结构无法恢复直立状态, 而具有变形能力的微结构则可以通过变形力恢复直立状态。随着刺激响应水凝胶技术的发展, 水凝胶强大的变形能力逐渐崭露头角。刺激响应水凝胶的性质会随着外界环境的变化而产生相应变化, 其中研究颇多的刺激类型是光^[16]、温度^[17]、pH值^[18-19]、离子^[20]和磁场^[21]等。由于水凝胶独特的变形能力和生物兼容性, 其被广泛应用于微机械、仿生执行器^[22]以及人造肌肉^[23-24]等领域。目前, 主要是通过各向异性设计使水凝胶产生结构变形的差异^[25-26]。如利用动态金属配体构建智能多色荧光聚合物水凝胶, 通过与纸结合构建双分子层软致动器, 在金属离子和温度的调控下水凝胶具有变色行为^[27]; 通过将热响应的氧化石墨烯 N-异丙基丙烯酰胺(NIPAM)水凝胶层和 pH 响应的聚乙烯亚胺水凝胶层结合, 得到可逆变形的具有定制三维形状的双层结构^[28]; 将丙烯酰胺酰胺层和 NIPAM 层构成复合层, 两层在低温和高温下具有相反行为, 基于此特性可以获得温度驱动的双层执行器^[29]; 此外, 通过对 pH 水凝胶的各向异性进行加工,

收稿日期: 2023-03-27; 修回日期: 2023-04-13; 录用日期: 2023-04-24; 网络首发日期: 2023-05-04

基金项目: 国家自然科学基金(61927814, 52175396)、合肥工业大学中央高校科研经费(JZ2022HGPA0312)

通信作者: *laozx@hfut.edu.cn

实现了多自由度形状转变的微执行器,这展现了 pH 水凝胶复杂的仿生变形能力^[30]。因此,将具有智能响应特性的水凝胶应用到 LPCS 技术中将为智能微纳结构制备提供新的思路。

本文利用飞秒激光加工温度响应水凝胶,在毛细力的驱动下可逆制备线接触的微结构,将 LPCS 技术和刺激响应水凝胶强大的变形能力结合,获得了具有定向运输能力的微执行器以及具有捕获、释放能力的微传感器。本文使用的水凝胶是温度响应水凝胶,该水凝胶的体积受温度变化影响,当溶液温度超过临界变形温度($\sim 32\text{ }^{\circ}\text{C}$)时,水凝胶体积收缩,反之,体积膨胀。利用飞秒激光加工参数的灵活可变性,改变水凝胶微结构两侧的扫描间距,导致水凝胶具有各向异性,在不同温度的溶液中会有互逆的变形方向。通过施加相反方向的条件,使水凝胶结构获得变形力,即使线接触

的微结构也能实现可逆组装。利用飞秒激光的真三维特性,制备了各种形状的可逆变形微执行器。此外,还通过毛细力驱动组装了丰富的图案和结构。最后利用水凝胶强大的变形能力,制备了可逆的微抓手传感器,展示了该策略在微机械、微传感等领域中的应用潜力。

2 加工系统和原理分析

2.1 加工系统

本文采用的飞秒激光双光子直写加工系统如图 1(a) 所示。实验中所使用的飞秒激光器的光源脉冲宽度为 75 fs,重复频率为 80 MHz,平均输出功率为 2.5 W,波长为 800 nm。使用的显微镜系统的数值孔径(NA)为 1.35。通过扫描振镜控制激光在 xy 平面内的移动,再通过压电台控制样品在 z 向上的精准移动,以此实现任何形状的三维打印。

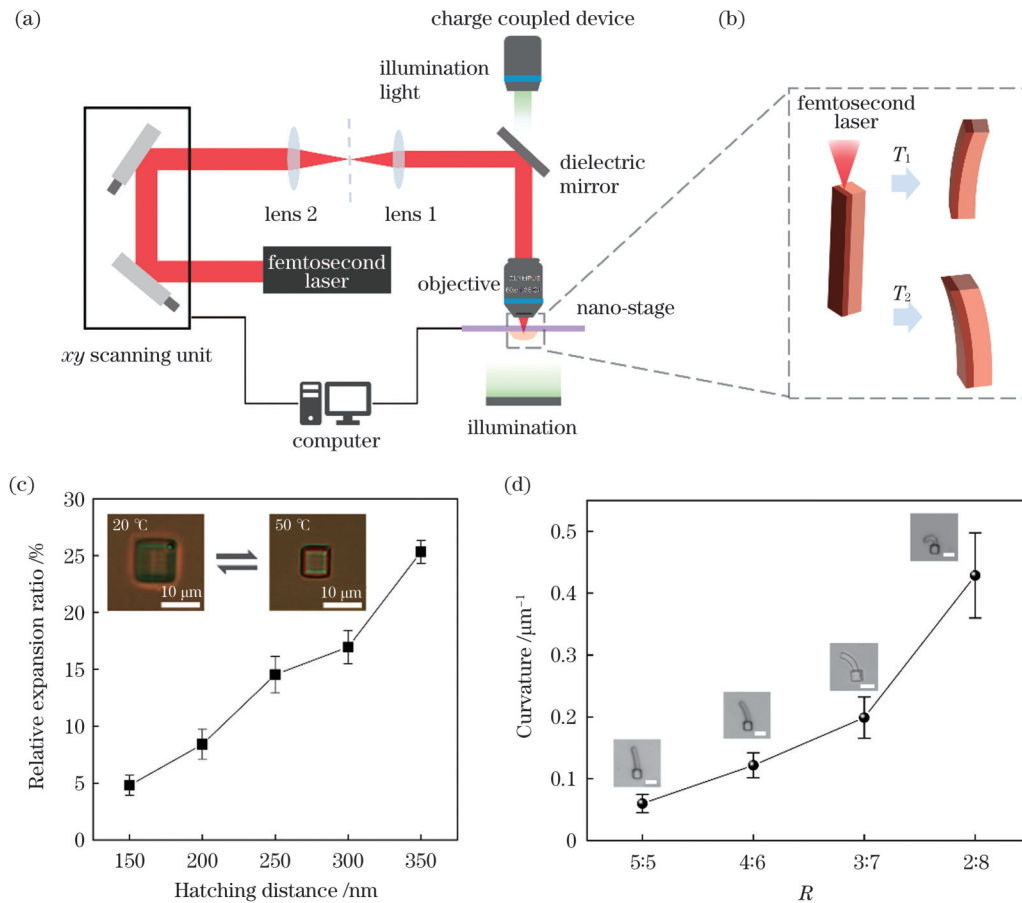


图 1 飞秒激光双光子加工。(a) 飞秒激光双光子加工系统光路示意图;(b) 飞秒激光双光子加工各向异性截面示意图;(c) 水凝胶微块的聚合程度和扫描间距的关系,其中插图是在 24 mW 能量下加工的方块变形的光学显微镜照片;(d) R 对水凝胶悬臂梁弯曲曲率的影响,其中插图是在相同能量下加工的具有不同 R 的悬臂梁的光学显微镜照片,比例尺为 $10\text{ }\mu\text{m}$

Fig. 1 Femtosecond laser two-photon processing. (a) Optical path diagram of femtosecond laser two-photon processing system; (b) diagram of anisotropic cross section by femtosecond laser two-photon processing; (c) relationship between degree of polymerization of hydrogel micro-block and hatching distance with optical micrograph of deformation of block processed at 24 mW energy shown in inset; (d) effect of R on bending curvature of hydrogel cantilever beam with optical micrographs of cantilever beams with different R at same energy shown in inset and scale bar of $10\text{ }\mu\text{m}$

激光经过扩束后到达扫描振镜,经过物镜聚焦到材料实现双光子聚合。所使用的材料为热敏性的水凝

胶,使用前需要在热板上烘 3~5 min。利用磁铁将滴有水凝胶的玻璃片固定在 z 向压电台上,并通过衰减

片调整适宜的能量。使用卤素灯照明样品并调整光照强度,移动压电平台,调整样品的位置,进行粗对焦,使加工的结构能够在电荷耦合器件(CCD)中成像并进行后续的实时观测,最后通过软件进行细对焦并在焦面处加工。将加工完毕的样品放入乙醇中显影10 min,去除掉未被聚合的部分,即可得到所需的结构。本套系统通过软件可以控制加工的曝光时间和扫描速度。

2.2 各向异性微结构的设计原理

实验中所使用的水凝胶为温度响应水凝胶(NIPAM),其内部含有亲水基团和疏水基团,温度的改变会影响这些基团和水分子的相互作用,从而使得水凝胶孔隙发生变化,导致体积的收缩/膨胀。当温度低于水凝胶的临界变形温度(T_c)时,聚合物网络中的亲水基团和水分子之间发生强氢键作用,水凝胶展现了较好的亲水性,因此水凝胶体积膨胀;当温度升高且高于水凝胶的临界变形温度时,氢键作用减弱,疏水基团的疏水作用加强并成为主导,因此水凝胶体积收缩^[31]。

在实验中发现,激光参数会对水凝胶的膨胀/收缩程度产生一定的影响,如加工能量、激光扫描间距、曝光时间等。加工能量越高,水凝胶的聚合程度越高,水凝胶的刚性越大,导致变形困难;反之水凝胶的聚合程度越低,变形程度越低。扫描间距的大小也会影响水凝胶结构的聚合程度,由于激光光斑本身是一个椭球体,其加工的位置也会对周围一定区域内的结构产生影响。当扫描间距较大时,受到影响的区域小,水凝胶的聚合程度较低,变形较大;反之变形较小。而曝光时间越长,水凝胶的聚合程度也会越高;曝光时间越短,聚合程度则越低。

本文系统没有能量控制器件,每加工一个结构,就需要手动调整相邻部分结构的加工能量,重复操作,无法保证一致性。其次,改变曝光时间的方式可能会产生过度曝光,从而影响结构的加工质量。根据我们的实验经验,曝光时间对结构刚度的影响是非线性的。对于智能响应水凝胶材料而言,如果单点曝光时间过长,可能会造成材料溶液升温,产生气泡,破坏结构。改变扫描间距的加工方式的灵活性比较高,通过控制激光焦点的三维空间坐标,可以实现不同的加工间距。

因此,本实验通过控制微结构两侧的扫描间距来实现各向异性截面。如图1(c)所示,我们探究了扫描间距对水凝胶聚合程度的影响,可以发现,随着扫描间距的增大,水凝胶的收缩率增大。为了获得较为理想的变形,我们选择收缩率差异较大的150 nm和350 nm的扫描间距。在曝光时间和加工能量固定的情况下,两侧分别采用150 nm和350 nm的扫描间距,如图1(b)所示,颜色较深的区域采用150 nm的扫描间距,而颜色较浅的区域采用350 nm的扫描间距。这里

两侧的宽度也有差异,当聚合程度高的一侧的宽度较大时,即使存在各向异性的差异,微结构的弯曲程度也不明显。图1(d)展示了不同扫描间距区域的宽度比(R)对结构曲率的影响。随着 R 的减小,悬臂梁的曲率增大,因此弯曲程度逐渐增大。当 R 为3:7时,弯曲曲率达到 $0.2 \mu\text{m}^{-1}$;当 R 达到2:8时,弯曲曲率超过 $0.4 \mu\text{m}^{-1}$,但是加工的微结构的表面形貌较为粗糙。这里选定聚合程度高和聚合程度低的区域宽度比是3:7。图1(b)中 T_1 是高于 T_c 的温度,在该温度下,水凝胶整体处于收缩的状态,扫描间距小的区域相对于扫描间距大的区域,收缩较小,因此结构会朝扫描间距大的一侧弯曲。而 T_2 是低于 T_c 的温度,此时水凝胶整体处于膨胀状态,但是扫描间距小的区域的膨胀程度小,所以此时结构会朝扫描间距小的一侧弯曲。因此,通过图1(b)可以看出,微结构存在两个弯曲方向。水凝胶在不同温度对应不同状态(膨胀/收缩),所以两次弯曲并不是镜像对称的,高温时微结构整体尺寸要小于低温时,并且微结构弯曲的曲率也相差了一个量级。

3 实验过程和结果分析

飞秒激光加工具备灵活性和真三维的特性,可以实现任意轨迹的加工,并且加工材料的范围比较广,如水凝胶、光刻胶^[32]、铈酸锂^[33]以及非晶合金^[34]等。实验中采用的激光加工能量为24 mW,曝光时间为800 μs 。通过滴加不同温度的去离子水来改变溶液环境。如图2(a)所示,利用各向异性截面设计的1-手臂微结构,手臂长度为30 μm ,在低于 T_c 和高于 T_c 的溶液环境下具有相反方向的弯曲变形,且具有良好的可逆性,响应的时间仅为200 ms。接下来,对水凝胶手臂的运输能力进行了测试,如图2(b)、(c)所示,在每一个长度为40 μm 的水凝胶手臂的末端,利用光刻胶材料加工出截面尺寸为10 $\mu\text{m} \times 10 \mu\text{m}$ 的矩形块,受不同温度溶液的刺激,手臂均有相反方向的弯曲变形,均可拉动刚性较大的光刻胶方块,通过控制加工的能量和曝光时间,可以实现微物体的定向移动。其中,图2(b)是2-手臂微结构,图2(c)是6-手臂微结构。当继续增大微物体的体积时,设计了截面尺寸为10 $\mu\text{m} \times 20 \mu\text{m}$ 的矩形块,此时,单根手臂无法推动物体移动,我们在同侧设计了两个手臂,如图2(d)所示。当结构处于低温环境中时,手臂膨胀时的变形不足以推动物体的移动,但当结构处于高温环境中时,手臂的收缩变形可以推动物体移动。

前文通过各种形态微手臂的设计展现了飞秒激光制备三维结构的灵活性,为了探究LPCS技术制备微结构的高效性,设计了大面积微结构的组装阵列,如图3所示。各向异性微结构的分布设计如图3(a)所示,插图表明了单元体内各向异性微板的分布设计。在常温(低于 T_c)下组装成的组装体

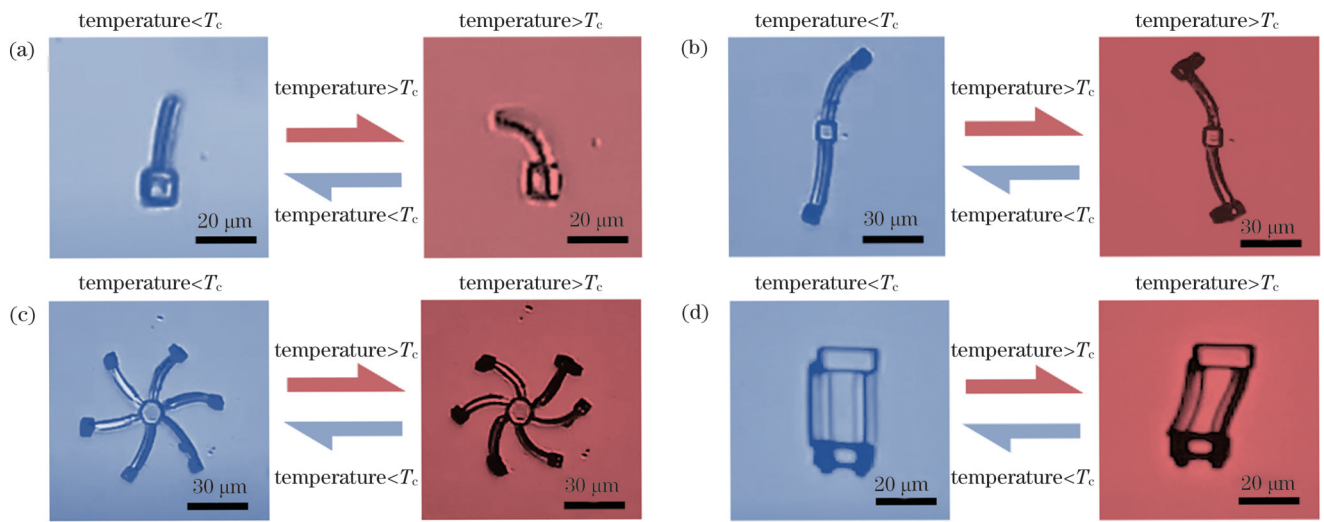


图 2 具备双向运动的微执行器。(a)1-手臂微结构;(b)2-手臂微结构;(c)6-手臂微结构;(d)同侧2-手臂微结构
 Fig. 2 Micro-actuators with bidirectional motion. (a) 1-arm microstructure; (b) 2-arm microstructure; (c) 6-arm microstructure; (d) ipsilateral 2-arm microstructure

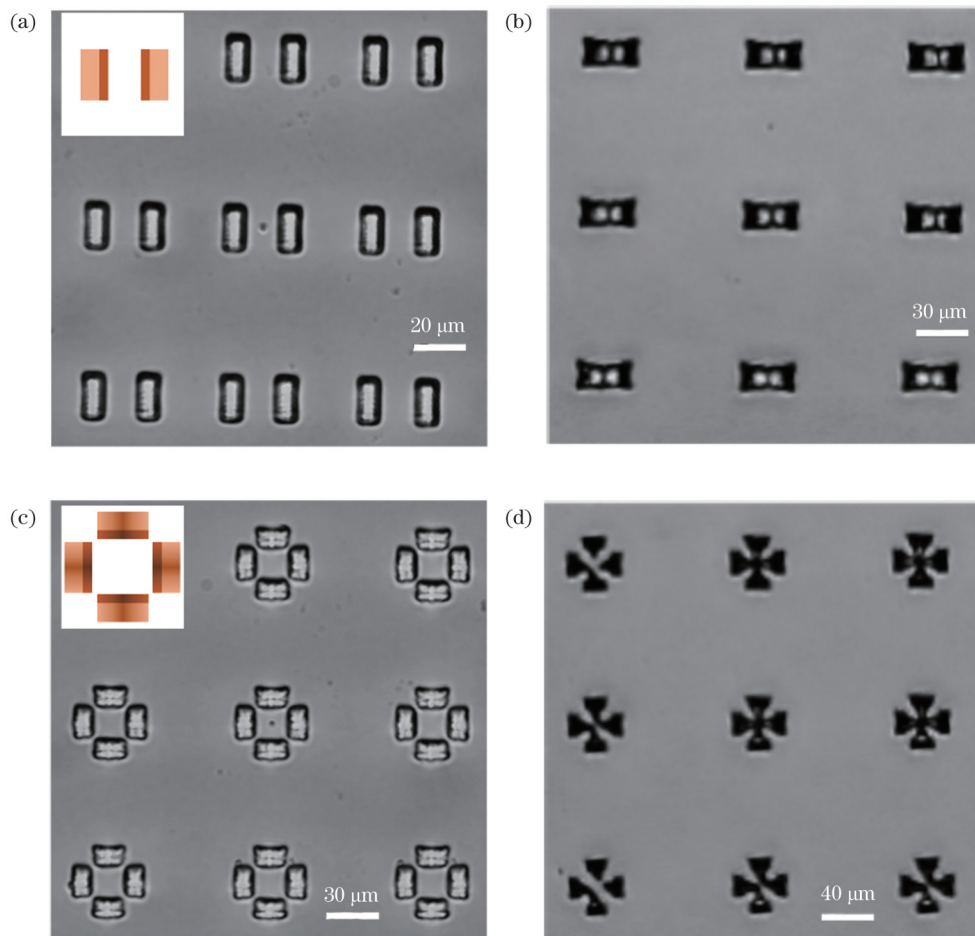


图 3 常温下 LPCS 技术制备的微组装体。(a) 打印的各向异性水凝胶微板结构在溶液中的光学显微镜图片, 其中插图是微板结构的各向异性截面设计;(b) 自组制备的线接触微板结构;(c) 打印的各向异性水凝胶四叶草结构在溶液中的光学显微镜图片, 其中插图是四叶草结构的各向异性截面设计;(d) 自组制备的多点接触的四叶草结构

Fig. 3 Micro-assemblies prepared by LPCS technology at room temperature. (a) Optical micrograph of printed anisotropic hydrogel microplates in solution with anisotropic cross-section design of microplate shown in inset; (b) wire contact microplate prepared by self-assembly; (c) optical micrograph of printed anisotropic hydrogel four-leaf clover in solution with anisotropic cross-section design of four-leaf clover shown in inset; (d) multi-contact four-leaf clover prepared by self-assembly

如图 3(b) 所示,其中,微板顶部接触为线接触,接触面积较大,此时的范德瓦耳斯力远大于点接触时的范德瓦耳斯力。此外,由于常温下上述设计的微柱是向单元内部弯曲的,因此通过调控单元内微板对的间距,可以获得不同高度的组装体,相对传统 LPCS 制备,其对空间分布的严格性要求降低。设计了纵截面是等腰三角形的三角柱结构(图 3(c)),通过图 3(c)中插图所示的空间排布,组装成图 3(d)所示的四叶草结构,由于每根微柱顶部都和其他三个微柱接触,故为多点接触。此外,由于微柱顶部尖细柔软,组装后四根微柱顶部会相互缠绕,也可以看作是线接触或面接触。因此,利用 LPCS 可以制备出多点接触或者线接触的微组装体。

传统的 LPCS 技术同样可以制备出多点接触和线接触的组装单元体,如超长尺寸的仿生毛细管通道、仿生微型抓手等。组装的微结构的接触区域的面

积过大,导致范德瓦耳斯力过大,制备的微功能器件等不具备可逆性,大大限制了结构的应用范围。如图 4(a)、(c)所示,分别利用温度响应水凝胶和液态光刻胶制备了微单元体,两者在毛细力驱动下均可组装成功,组装后为线接触。不同的是,将水凝胶制备的微组装体放入到高温的溶液中,由于反向的变形力,此时组装体恢复站立状态,而液态光刻胶制备的微组装体被浸入到溶液中后并不能解除组装形态,如图 4(b)、(d)所示。这里液态光刻胶聚合后的刚度远大于水凝胶聚合后的刚度,因此光刻胶微结构的弹性力远大于水凝胶微结构。组装完毕微结构保持稳定的原因是弹性力和范德瓦耳斯力之间的博弈,具有较大弹性力的光刻胶微结构在浸入溶液后不能恢复站立状态,而具有较小弹性力的水凝胶微结构在浸入溶液后可以恢复站立状态,即水凝胶在温度刺激下变形而产生了变形力。

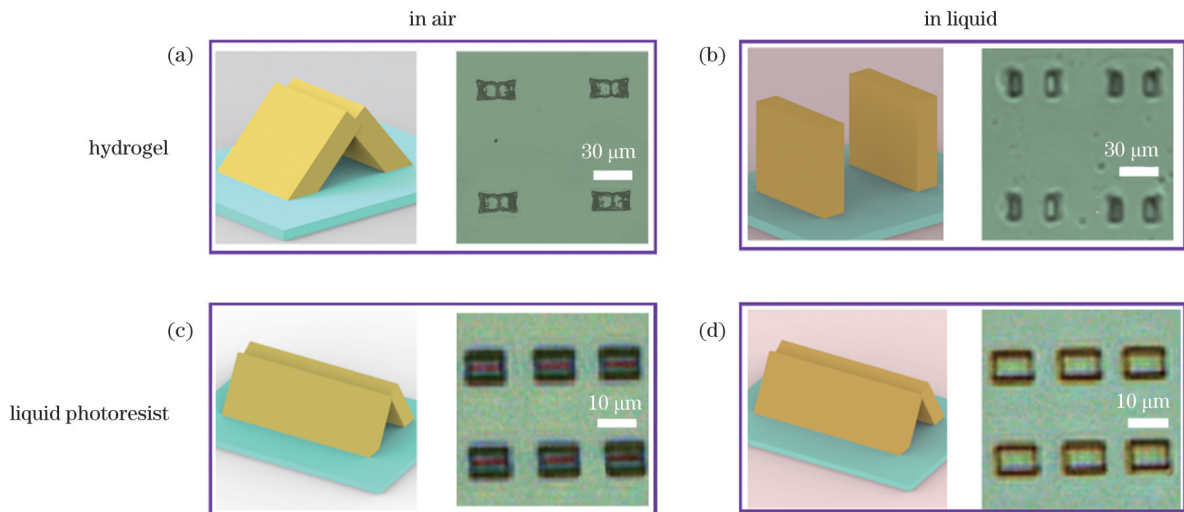


图 4 不同材料制备的线接触结构的可逆性分析。(a) 组装后的水凝胶微结构的示意图和光学显微镜照片;(b) 将图 4(a) 中结构浸入溶液后的示意图和光学显微镜照片;(c) 组装后的液态光刻胶微结构的示意图和光学显微镜照片;(d) 将图 4(c) 中结构浸入溶液后的示意图和光学显微镜照片

Fig. 4 Reversibility analysis of line contact microstructures prepared with different materials. (a) Diagram and optical micrograph of assembled hydrogel microstructures; (b) diagram and optical micrograph of microstructures in Fig. 4(a) after immersion in solution; (c) diagram and optical micrograph of assembled liquid photoresist microstructures; (d) diagram and optical micrograph of microstructures in Fig. 4(c) after immersion in solution

随后我们利用温度响应水凝胶在高温下的显著收缩特性,制备了具有可逆组装特性的线接触的微抓手,并探究了其在微传感领域中的应用。如图 5(a) 所示,该结构通过溶液(温度为 T_2)挥发并借助毛细力驱动自组装,实现闭合,可用于捕获物体;该结构通过感知环境的变化(溶液温度升为 T_1),实现展开,做出释放的行为。值得注意的是,这里的 T_1 、 T_2 不是一个准确的温度值,而是一个温度范围, T_1 低于临界变形温度, T_2 高于临界变形温度。类似于图 3(c) 所示的各向异性截面设计,本文设计了高度为 $30\ \mu\text{m}$ 的微传感器结构。将打印好的微传感器放置在温度低于 T_c 的常温

溶液中,微柱会朝内轻微弯曲(图 5(b))。图 5(c) 展现的是组装后的微传感器的俯视图,有比较好的封闭性。从电镜图(SEM)可以看出,组装体不仅顶部存在接触,侧边也有线接触,大大增加了各个微柱之间的范德瓦耳斯力。此时,将该传感器置于温度高于 T_c 的溶液中,如图 5(d) 所示,水凝胶吸热收缩,产生了反向的变形力,拉动微柱向外弯曲,可以明显看出微传感器的各个“手臂”向外展开。当溶液温度冷却至室温时,“手臂”会再次膨胀向内轻微弯曲,展现了可逆的过程。此外,水凝胶微传感器具有良好的抗疲劳性能,因此可以重复使用。

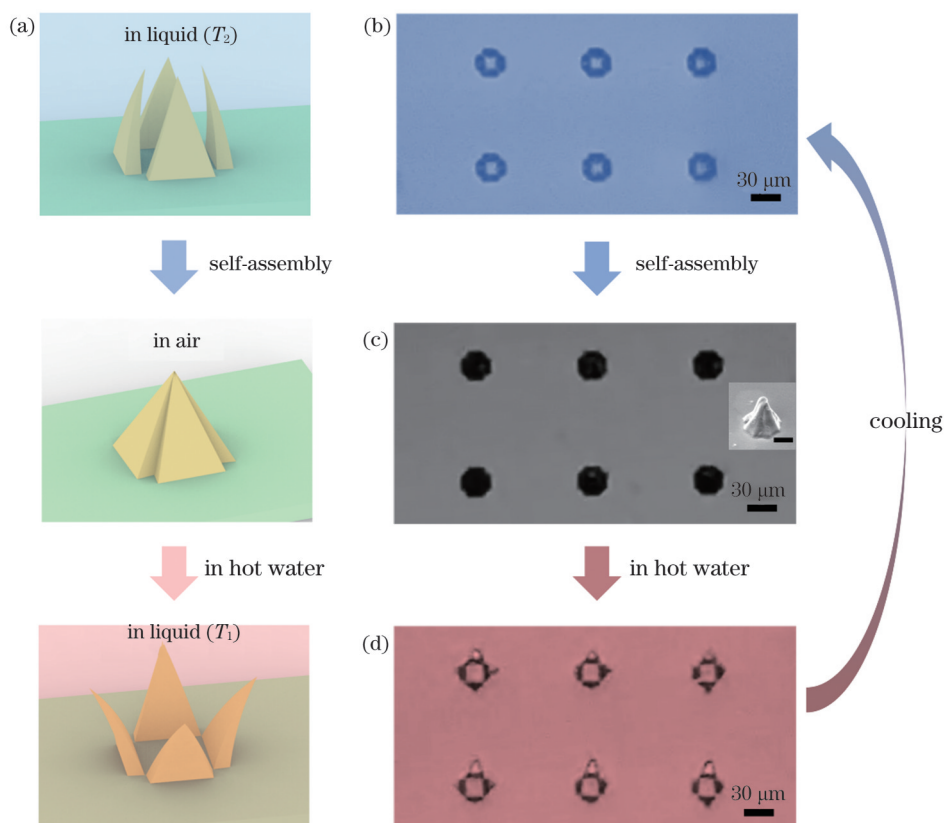


图5 微传感器的可逆制备过程。(a)微传感器可逆驱动的示意图;(b)微传感器在常温溶液中的光学显微镜照片;(c)组装后的微传感器的光学显微镜照片,其中插图为电镜图,比例尺为 $20\ \mu\text{m}$;(d)微传感器在温度高于 T_c 的溶液中的光学显微镜照片

Fig. 5 Reversible preparation of microsensors. (a) Diagram of reversible drive of microsensors; (b) optical micrograph of microsensors in solution at room temperature; (c) optical micrograph of assembled microsensors with SEM shown in inset and scale bar of $20\ \mu\text{m}$; (d) optical micrograph of microsensors in solution at temperature higher than T_c .

4 结 论

利用飞秒激光打印各向异性的水凝胶微结构,通过温度调节控制其运动方向,实现对微物体的定向运输。将激光打印的水凝胶结构和毛细力驱动自组装结合,获得了丰富的微图案。进一步证明了飞秒激光双光子加工的灵活性及其与毛细力驱动结合制备层级结构的便捷性。更重要的是,利用温度响应水凝胶的变形特性,在毛细力的驱动下可逆制备线接触的微传感器。通过高温下水凝胶显著收缩产生的变形力,实现了封闭微抓手的展开,解决了以往LPCS方法制备的线接触微结构组装行为的不可逆问题。通过对周围环境的感应,微结构实现了关闭和展开,大大丰富了LPCS技术在传感器领域中的应用。

参 考 文 献

- [1] Maruo S, Ikuta K, Korogi H. Submicron manipulation tools driven by light in a liquid[J]. Applied Physics Letters, 2003, 82(1): 133-135.
- [2] Langer G, Brodoceanu D, Bäuerle D. Femtosecond laser fabrication of apertures on two-dimensional microlens arrays[J]. Applied Physics Letters, 2006, 89(26): 261104.
- [3] Chen Q D, Wu D, Niu L G, et al. Phase lenses and mirrors created by laser micromanufacturing via two-photon photopolymerization[J]. Applied Physics Letters, 2007, 91(17): 171105.
- [4] McDonald J P, Mistry V R, Ray K E, et al. Femtosecond pulsed laser direct write production of nano- and microfluidic channels[J]. Applied Physics Letters, 2006, 88(18): 183113.
- [5] Wu D, Ding Y L, Zhang Y X, et al. 3D microfluidic cloth-based analytical devices on a single piece of cloth by one-step laser hydrophilicity modification[J]. Lab on a Chip, 2021, 21(24): 4805-4813.
- [6] Xin C, Jin D D, Hu Y L, et al. Environmentally adaptive shape-morphing microrobots for localized cancer cell treatment[J]. ACS Nano, 2021, 15(11): 18048-18059.
- [7] Armani A M, Kulkarni R P, Fraser S E, et al. Label-free, single-molecule detection with optical microcavities[J]. Science, 2007, 317(5839): 783-787.
- [8] Asbahi M, Mehraeen S, Wang F K, et al. Large area directed self-assembly of sub-10 nm particles with single particle positioning resolution[J]. Nano Letters, 2015, 15(9): 6066-6070.
- [9] Chandra D, Yang S. Capillary-force-induced clustering of micropillar arrays: is it caused by isolated capillary bridges or by the lateral capillary meniscus interaction force?[J]. Langmuir, 2009, 25(18): 10430-10434.
- [10] Duan H G, Berggren K K. Directed self-assembly at the 10 nm scale by using capillary force-induced nanocoheion[J]. Nano Letters, 2010, 10(9): 3710-3716.
- [11] Hu Y L, Lao Z X, Cumming B P, et al. Laser printing hierarchical structures with the aid of controlled capillary-driven self-assembly[J]. Proceedings of the National Academy of Sciences of the United States of America, 2015, 112(22): 6876-6881.
- [12] Lao Z X, Pan D, Yuan H W, et al. Mechanical-tunable capillary-

- force-driven self-assembled hierarchical structures on soft substrate [J]. *ACS Nano*, 2018, 12(10): 10142-10150.
- [13] Lao Z X, Zheng Y Y, Dai Y C, et al. Nanogap plasmonic structures fabricated by switchable capillary-force driven self-assembly for localized sensing of anticancer medicines with microfluidic SERS[J]. *Advanced Functional Materials*, 2020, 30(15): 1909467.
- [14] 刘絮飞, 韩丹翔, 郭慧, 等. 基于飞秒激光微纳结构化聚四氟乙烯材料的表面增强拉曼散射基底[J]. *激光与光电子学进展*, 2021, 58(23): 2314011.
- Liu X F, Han D A, Guo H, et al. Surface enhanced Raman scattering substrates based on femtosecond laser structured polytetrafluoroethylene[J]. *Laser & Optoelectronics Progress*, 2021, 58(23): 2314011.
- [15] Lao Z X, Hu Y L, Pan D, et al. Self-sealed bionic long microchannels with thin walls and designable nanoholes prepared by line-contact capillary-force assembly[J]. *Small*, 2017, 13(23): 1603957.
- [16] Sutton A, Shirman T, Timonen J V I, et al. Photothermally triggered actuation of hybrid materials as a new platform for *in vitro* cell manipulation[J]. *Nature Communications*, 2017, 8: 14700.
- [17] Zarzar L D, Kim P, Kolle M, et al. Direct writing and actuation of three-dimensionally patterned hydrogel pads on micropillar supports [J]. *Angewandte Chemie*, 2011, 123(40): 9528-9532.
- [18] 孙锐, 王重宇, 胡衍雷, 等. 飞秒激光加工水凝胶双面神微柱及其应用[J]. *中国激光*, 2019, 46(9): 0902001.
- Sun R, Wang Z Y, Hu Y L, et al. Processing and application of hydrogel Janus micropillars based on femtosecond laser[J]. *Chinese Journal of Lasers*, 2019, 46(9): 0902001.
- [19] Jin D D, Chen Q Y, Huang T Y, et al. Four-dimensional direct laser writing of reconfigurable compound micromachines[J]. *Materials Today*, 2020, 32: 19-25.
- [20] Ren Y Y, Liu Z Y, Jin G Q, et al. Electric-field-induced gradient ionogels for highly sensitive, broad-range-response, and freeze/heat-resistant ionic fingers[J]. *Advanced Materials*, 2021, 33(12): 2008486.
- [21] Saadli M, Braunmiller D L, Mourran A, et al. Thermally and magnetically programmable hydrogel microactuators[J]. *Small*, 2023, 19(16): 2207035.
- [22] Zhao Y S, Lo C Y, Ruan L C, et al. Somatosensory actuator based on stretchable conductive photothermally responsive hydrogel [J]. *Science Robotics*, 2021, 6(53): eabd5483.
- [23] Zhu Q L, Du C, Dai Y H, et al. Light-steered locomotion of muscle-like hydrogel by self-coordinated shape change and friction modulation[J]. *Nature Communications*, 2020, 11: 5166.
- [24] Ge G, Lu Y, Qu X Y, et al. Muscle-inspired self-healing hydrogels for strain and temperature sensor[J]. *ACS Nano*, 2020, 14(1): 218-228.
- [25] Lee M R, Phang I Y, Cui Y, et al. Shape-shifting 3D protein microstructures with programmable directionality via quantitative nanoscale stiffness modulation[J]. *Small*, 2015, 11(6): 740-748.
- [26] Amjadi M, Sitti M. High-performance multiresponsive paper actuators[J]. *ACS Nano*, 2016, 10(11): 10202-10210.
- [27] Wei S X, Lu W, Le X X, et al. Bioinspired synergistic fluorescence-color-switchable polymeric hydrogel actuators[J]. *Angewandte Chemie International Edition*, 2019, 58(45): 16243-16251.
- [28] Ma C X, Lu W, Yang X X, et al. Bioinspired anisotropic hydrogel actuators with on-off switchable and color-tunable fluorescence behaviors[J]. *Advanced Functional Materials*, 2018, 28(7): 1704568.
- [29] Li J, Ma Q Y, Xu Y, et al. Highly bidirectional bendable actuator engineered by LCST-UCST bilayer hydrogel with enhanced interface[J]. *ACS Applied Materials & Interfaces*, 2020, 12(49): 55290-55298.
- [30] Hu Y L, Wang Z Y, Jin D D, et al. Botanical-inspired 4D printing of hydrogel at the microscale[J]. *Advanced Functional Materials*, 2020, 30(4): 1907377.
- [31] Pasparakis G, Tsitsilianis C. LCST polymers: thermoresponsive nanostructured assemblies towards bioapplications[J]. *Polymer*, 2020, 211: 123146.
- [32] 胡昕宇, 马卓晨, 韩冰, 等. 飞秒激光制备蛋白质智能软体执行器[J]. *中国激光*, 2021, 48(14): 1402001.
- Hu X Y, Ma Z C, Han B, et al. Femtosecond laser fabrication of protein-based smart soft actuators[J]. *Chinese Journal of Lasers*, 2021, 48(14): 1402001.
- [33] 乔玲玲, 汪旻, 伍荣波, 等. 超低损耗铌酸锂光子学[J]. *光学学报*, 2021, 41(8): 0823012.
- Qiao L L, Wang M, Wu R B, et al. Ultra-low loss lithium niobate photonics[J]. *Acta Optica Sinica*, 2021, 41(8): 0823012.
- [34] 姚燕生, 陈锐, 葛张森, 等. Zr基非晶合金激光加工表面羟基磷酸灰石沉积特性研究[J]. *中国激光*, 2022, 49(10): 1002604.
- Yao Y S, Chen R, Ge Z S, et al. Hydroxyapatite deposition properties on laser processed surface of zirconium-based amorphous alloy[J]. *Chinese Journal of Lasers*, 2022, 49(10): 1002604.

Reversible Self-Assembly of Temperature-Driven Femtosecond Laser Printed Microstructures

Ni Caiding¹, Lao Zhaoxin^{2*}, Ren Zhongguo¹, Chen Chao³, Wu Dong¹

¹*School of Engineering Science, University of Science and Technology of China, Hefei 230026, Anhui, China;*

²*Anhui Province Key Laboratory of Measuring Theory and Precision Instrument, School of Instrument Science and Optoelectronic Engineering, Hefei University of Technology, Hefei 230009, Anhui, China;*

³*Department of Materials Physics and New Energy Device, School of Materials Science and Engineering, Hefei University of Technology, Hefei 230009, Anhui, China*

Abstract

Objective Template-guided capillary force-driven self-assembly technology is increasingly being considered as an alternative for fabricating a range of micro/nanostructures. Because of the advantages of rapid preparation of large-area and controllable complex hierarchical microstructures, the combination of femtosecond laser and capillary force-driven assembly (LPCS) technology has become an attractive method. In the LPCS method, the stability of the microstructure depends on the competition between the contact force, e. g., the van der Waals force, and elastic force of the microstructure after self-assembly. The contact force between microstructures

is positively correlated with the contact area of the microstructure. A larger contact area corresponds to the larger van der Waals force and more stable assembly. When the contact area is greater than the critical value, the microstructure assembly behavior is irreversible. In our previous research, we found that microstructures with linear contact, such as microwalls, or even microstructures with surface contact could not be restored to the upright state after immersion in a liquid because of the large contact area after assembly, which greatly limits the application range of microstructures. In this study, the reversible self-assembly of linear contact microstructures prepared by LPCS is realized by taking advantage of the significant deformation ability of temperature-responsive hydrogels.

Methods In this study, the temperature-responsive hydrogel is mainly composed of N-isopropylacrylamide, acrylamide, and phosphine oxide, where N-isopropylacrylamide is the monomer, acrylamide is the crosslinking agent, and phosphine oxide is the photoinitiator. We successively put the 400 mg N-isopropylacrylamide, 30 mg acrylamide, 30 mg phosphine oxide, and 450 μL glycol into a bottle and then place the bottle in a water bath at 50 $^{\circ}\text{C}$ for ultrasound. Finally, the 50 mg polyethylene pyrrolidone is added as a viscosifier. The femtosecond laser source used in the experiment has a pulse width of 75 fs, repetition frequency of 80 MHz, average output power of 2.5 W, and wavelength of 800 nm. The microscope system consists of a lens with a numerical aperture of 1.35. A scanning galvanometer is used to control the movement of the laser in the xy plane, and a nanostage is used to control the precise movement of the sample in the z direction to realize 3D printing of any shape. During processing, the measured average laser power is 24 mW, and the hatching distances used for anisotropic microstructures are 150 nm and 350 nm. After processing, the samples are placed in a developer (ethanol) for 10 min to remove any unpolymerized hydrogel.

Results and Discussions We investigate the effects of different hatching distances (HDs) on the degree of hydrogel polymerization. With an increase in HD, the shrinkage rate of the hydrogel increases. To achieve significant deformation and good surface appearance, HDs of 150 nm and 350 nm and their area width ratio of 3:7 are selected, as shown in Figs. 1(c) and (d). Anisotropic arm microstructures with a length of 30 μm are designed as shown in Fig. 2. When the solution temperature is lower or higher than the critical temperature, arm bending deformation occurs in the opposite direction and exhibits good reversibility. In addition, the arm shows good transportation ability. As shown in Fig. 3, we apply LPCS technology to temperature-responsive hydrogels to prepare a variety of assembly patterns. Compared with the traditional LPCS preparation, the requirements for spatial distribution are reduced. Finally, Figure 5 shows that based on the remarkable shrinkage property of temperature-responsive hydrogels at high temperatures, linear contact microgrippers with reversible assembly are prepared, and their applications in the field of microsensing are explored. Microgrippers with good airtightness and fatigue resistance can be repeatedly used.

Conclusions In this study, anisotropic hydrogel microstructures are printed using a femtosecond laser, and the direction of their movement is controlled by temperature regulation to realize the directional transport of micro-objects. Second, laser-printed hydrogel microstructures are combined with capillary force-driven self-assembly to obtain rich micropatterns. This further demonstrates the flexibility of femtosecond laser two-photon processing and the convenience of preparing hierarchical microstructures combined with capillary force-driven self-assembly. More importantly, microgrippers with line contacts can be reversibly prepared using the deformation characteristics of temperature-responsive hydrogels. The closed microgrippers can be opened through the deformation force generated by the significant shrinkage of the hydrogel at high temperatures, which resolves the irreversibility of the assembly behavior of line contact microstructures prepared by the previous LPCS method. By sensing the surrounding environment, the microstructures can be closed and opened, greatly enriching the application of LPCS technology in the field of sensors.

Key words laser technique; femtosecond laser; two-photon polymerization; capillary forces; self-assembly; temperature response